NASA TECHNICAL
MEMORANDUM

CASE FILE
COPY

A COMPACT 90 KILOWATT ELECTRIC HEAT SOURCE
FOR HEATING INERT GASES TO 1700° F

by Robert P. Macosko, Henry R. Block, Stacy Lumannick, and Carl W. Richter
Lewis Research Center
Cleveland, Ohio

This information is being published in preliminary
form in order to expedite its early release.

A COMPACT 90 KILOWATT ELECTRIC HEAT SOURCE

FOR HEATING INERT GASES TO 1700° F

by Robert P. Macosko, Henry B. Block,

Stacy Lumannick, Carl W. Richter

Lewis Research Center
Cleveland, Ohio

March 1970

ABSTRACT

A compact electric heat source was designed and fabricated at the Lewis Research Center for use in NASA Brayton power system testing. The heat source was designed to operate with a system gas of either krypton or a helium-xenon mixture at gas outlet temperatures ranging from 1250 to 1650° F. When used with a 208-volt 3-phase electrical supply, the heat source will provide up to 90 kilowatts of thermal power to the gas.

A COMPACT 90 KILOWATT ELECTRIC HEAT SOURCE

FOR HEATING INERT GASES TO 1700° F

by Robert P. Macosko, Henry B. Block

Stacy Lumannick, & Carl W. Richter

Lewis Research Center

SUMMARY

A compact electric heat source was designed and fabricated at the Lewis Research Center for use in NASA Brayton power system testing. The heat source was designed to operate with a system gas of either krypton or a helium-xenon mixture at gas outlet temperatures ranging from 1250 to 1650° F. When used with a 208-volt 3-phase electrical supply, the heat source will provide up to 90 kilowatts of thermal power to the gas.

The heat source was operated for 225 hours with krypton gas for a wide range of gas flows, power levels, and gas outlet temperatures. The heat source performance very closely matched the predicted performance. The heating elements reached a maximum temperature of 1975° F at the exit zone of the core which was well below the established safe heating element temperature limit of 2100° F.

Static pressure losses through the heat source were low. The pressure drop was 0.20 percent of the heat source inlet absolute pressure at the maximum weight flow condition (1.7 lbs/sec).

INTRODUCTION

The need for power generating systems that can operate for one to five years in space has brought about the development of the NASA Brayton power system. This system operates on the Brayton thermodynamic cycle and uses an inert gas as the working fluid. The Brayton engine has been designed to operate with any one of three energy sources. These are an isotope, a nuclear reactor, or a solar collector. Since the use of these energy sources for preliminary system testing would complicate the task and increase cost, various types of electric energy sources have been employed by NASA in Brayton tests.

Two test systems (ref. 1 and 2) have used commercially available resistance heaters (forced-convection type). These units were large (approximately 8 in. diameter X 10 ft. long) and added a large amount of gas volume to the test system. The thermal response of these units was limited due to the large mass of the heaters and, in particular, the associated piping. Problems with internal shorting were experienced during power ramps where the element temerature exceeded 1950° F.

A radiant-type heat source (ref. 3) was designed for NASA for use in testing the Brayton system in a vacuum environment. This unit deteriorated during use such that system requirements could not be achieved. Polished-aluminum heat-lamp reflectors became coated with deposits that resulted in a gradual decrease in radiation heat transfer capability. Tungsten heating elements were substituted for the heat lamps and reflectors but this concept has not yet been fully tested.

Because of the limitations of and problems encountered with the above heaters and the unavailability of smaller units commercially, a compact forced-convection heat source was designed and constructed. This heat source was designed to operate with a system gas of either krypton or helium-xenon (83.8 molecular weight) at gas outlet temperatures ranging from 1250 to 1650° F. When used with a 208-volt 3-phase electrical supply, the heater will provide up to 90 kilowatts of thermal power. The heat source core was designed to operate with a low Reynolds number (500 to 2500). At a krypton gas flow of 1.7 lbs/sec the predicted pressure drop was 0.21 percent of the heat source inlet absolute pressure.

This report presents preliminary heat source performance data for a wide range of krypton gas flows, outlet temperatures, and power levels. A comparison of predicted and experimental performance is presented along with experimentally determined parameters that would aid the user in predicting the performance of the heat source when used with other inert gases. The data presented are also applicable to the design of other electric heaters that incorporate similar core geometry.

2

SYMBOLS

A   Exchanger total heat transfer area on one side; (ft^2)

A_C Exchanger minimum free-flow area; (ft^2)

A_{FR} Exchanger total frontal area; (ft^2)

Cp   Specific heat at constant pressure; (BTU/lb ^oF)

D   Hydraulic diameter; (ft)

f   Mean friction factor; defined by equation (9), Appendix A; dimensionless

G   Exchanger flow stream mass velocity (W/A_c); (lbs/sec ft^2)

g_c Gravity term = (32.2 (lbs/#)(ft/sec^2))

h   Unit conductance for thermal convection heat transfer; (BTU/(sec ft^2 ^oF))

j   Heat transfer factor $(N_{ST}N_{PR}{}^{2/3})$; dimensionless

k   Thermal conductivity; (BTU/(sec ft^2 ^oF)/FT)

N_{PR} Prandtl number $\left(\dfrac{\mu\, Cp}{k}\right)$; dimensionless

N_R Reynold's number $\left(\dfrac{GD}{\mu}\right)$; dimensionless

N_{ST} Stanton number $(h/G\, C_p)$; dimensionless

P   Pressure; $(\#/ft^2)$

Q   Electrical energy dissipated to gas; (BTU/sec)

q   Heat transfer rate; (BTU/sec)

R   Electrical resistance; ohms

V   Specific volume; (cu ft/lb)

W   Mass flow rate; (lbs/sec)

Δ Denotes difference

μ Dynamic viscosity; (#/ft sec)

ρ Electrical resistivity; (micro-ohm inches)

σ Ratio of free-flow area to frontal area (A_C /A_{FR}); dimensionless

SUBSCRIPTS

1   Heat exchanger core inlet

2   Heat exchanger core outlet

I   Inconel 600

in   Inlet

l   Local

LM   Log mean average

m   Mean conditions

N   Nickel 200

out   Outlet

t   Tube

FORCE AND MASS UNITS

lb   Denotes pounds mass in distinction to

\#   Denoting pounds force

DESCRIPTION OF HEAT SOURCE

The heat source is comprised of two basic components: the heat exchanger core; and the containment vessel. All materials used in the heat source are listed in Table I.

The heat source core is a staggered tube bank of 500 Inconel tubes having a 3/8-inch outer diameter and .065-inch wall thickness (fig. 1). The tubes are heated by passing current directly through the tube wall as opposed to conventional electric heaters that utilize an insulated nichrome wire inside of the tube. Each tube is 12.5 inches long and is supported on each end by a ceramic (alumina) header. Nickel pins were brazed into each end of the tubes to serve as electrical connectors. The braze material used had a melting point of $2250°$ F. The tubes were joined by nickel jumpers to form three independent series resistors of 166 tubes each. Two additional tubes, which were not connected electrically, were installed in the core to complete the tube pattern.

Figure 1 shows the tubes installed in the headers with nickel jumpers welded in place. The resistor banks (phases) were arranged as shown in figure 2. Gas flow is across and normal to the electrically heated tubes. The header and tube assembly (core) stands freely within the containment vessel. Baffles were utilized to direct the gas flow across the tube bank and to allow limited movement of the headers. This method of construction allows a good deal of freedom for thermal expansion within the core.

The core, excluding the headers, measures approximately 12 in. X 12 in. X 12 in. The containment vessel is a 21-inch diameter cylinder constructed of 1/2-inch Inconel plate (fig. 3). The large tubes protruding from the cylinder are electrical power lead and instrumentation ports. These ports were designed to be left uninsulated so that the ceramic feedthroughs at the ends would remain below $600°$ F during heater operation in ambient air. Six power leads (2 per phase) and 20 thermocouples were brought out through the ten ports (figs. 3 and 4).

Transition cones were attached to the gas inlet and outlet sides of the containment vessel primarily to provide proper flow distribution across the heater core. With the transitions installed, the overall length of the heat source was about 36 inches. Also shown in figure 4 are the four mounting points located on the heat source outlet cone.

6

Power is applied to each phase of the heater through stranded nickel leads surrounded by ceramic insulators (fig. 5). A nickel lead is constructed of 23 cables with each cable consisting of 65 strands of No. 30 AWG solid nickel wire. The cable ends were crimped into solid nickel terminals also shown in figure 5. The small terminal attaches to the heater core and the large terminal to the electrical feedthrough on the power port.

Neglecting the resistance of the leads and braze, the calculated resistance of each phase is approximately 1.5 ohms at heating-element operating temperatures of 1000 to 2000° F. Inconel 600 has a constant electrical resistivity over this temperature range (ref. 4).

For this test the three phases of the core were connected in a delta pattern. A maximum electrical power input to the heat source of 93 kilowatts (31 kW per phase) was possible with a 208-volt 3-phase power supply. Current per phase at this power level would be approximately 150 amperes.

Instrumentation

Twenty chromel-alumel (CA) thermocouples were installed on the heat source core for operation and performance evaluation (see fig. 2). Ten of these thermocouples were installed in the centers of selected tubes. The remaining ten thermocouples were attached to the nickel jumpers at selected locations in each of the phases. All of these internal thermocouples had stainless steel sheaths with the end junction seal welded to prevent external gas leakage. All of the thermocouples were insulated with ceramic (alumina) beads to prevent electrical shorting to ground inside the instrumentation ports. These 20 thermocouples were brought out from the core and brazed to ceramic feedthroughs on the four instrumentation ports.

Heater skin temperatures, and the electrical and instrumentation port temperatures were measured with CA thermocouples spot welded at selected locations. Heat source inlet and outlet gas temperatures were measured using CA immersion thermocouples.

Heater pressure drop was measured with a strain gauge type differential pressure transducer. After calibration, this type of instrument is capable of measuring pressure drop within .02 #/in^2.

Installation

Figure 6 is a schematic of the basic Brayton system with the electric heat source and associated subsystems.

The electric heat source was installed in the support structure as shown in figure 4. A dotted line was added to the photograph to represent the heat source inlet and outlet piping which were not installed at the time this photo was taken.

The heat source and its associated piping were wrapped with high temperature quartz blanket insulation to a thickness of approximately six inches (fig. 7). A 12-inch length on each electrical and instrumentation port was left uninsulated to keep the ceramic feed-throughs from overheating. In addition, two small blowers were installed below the feedthrough ports to provide good air circulation.

Power to the heat source was regulated by a 3-phase SCR type of power controller. This unit provided both manual and set-point modes of operation. At 208 volts line-to-line, the power controller was rated at a total of 90 kVA.

A calibrated venturi for measuring gas mass flow rate was installed in the system piping between the Brayton heat exchanger unit and the heat source inlet.

Six of the heater core thermocouples were monitored on panel meter relays in the control room. Three of these were on the tubes of the exit phase, two on the exit phase nickel jumpers, and one on a middle-phase tube. In the event that any of these temperatures exceeded 2100° F, an automatic shutdown of the heat source was initiated via the meter relays.

A digital data acquisition system located in the control room monitored and recorded all heat source internal thermocouples, the gas inlet and outlet temperatures, gas mass flow rate, and heat source pressure information. Other heater data were recorded manually from meters in the control room and in the test cell.

OPERATING PROCEDURE

Preheat

Prior to first applying electrical power to the heat source, the Brayton system was evacuated below 0.1 torr. About 5 kW was then applied to raise the heater core to an average temperature of about 300° F. The heat source was maintained at this temperature and pressure for about ten hours to remove any moisture that may have been absorbed by the ceramic headers. The system was then charged with krypton gas to a pressure of approximately 14 psia.

Approximately 10 kW was applied to the heater to raise the core hot-spot temperature to 1800° F. (The core average temperature stabilized at 1500° F after approximately three hours.)

System Startup

The Brayton system was started by injecting krypton gas into the heat source at .35 lbs/sec and 70° F. The heat source controller was set for 30 kilowatts input (manual mode). After approximately 20 seconds, the gas exiting the heater had reached 1150° F. The controller was then switched over to set-point mode and the heater outlet temperature was increased to the desired level. Maximum heater outlet gas temperature for this test was 1650° F.

It should be noted that within a few seconds after gas injection, the heat source inlet temperature started to increase due to pre-heating in the recuperator.

Performance

The heat source was operated for approximately 225 hours. Approximately 50 hours of this time were at a krypton gas outlet temperature of 1650° F. During the test, data was acquired at heater outlet temperatures as low as 1250° F. The gas flow rate through the heat source varied from approximately .4 to 1.7 lbs/sec and the electrical power input varied from roughly 20 to 60 kilowatts.

A thermal map of the heat source at a typical operating condition is shown in figure 8.

Thermocouples were located on the inlet, middle, and exit tubes of the core as well as on various areas of the containment vessel skin. In general, the temperatures at the centers of the heating elements ran hotter than the temperatures of the nickel jumpers at a particular zone. The jumper temperatures at the inlet zone consistently ran hotter than the heating element centers. This was due to heat transfer to the jumpers from the static gas surrounding them. For all test conditions the centers of the exit tubes represented the hottest area in the core. The hottest tube reached a temperature of 1975° F. The power and instrumentation port temperatures did not exceed 200° F during the test.

Figure 9 is a comparison of actual heat source performance factors (j and f) with the predicted performance factors presented in reference 5, figure 50. The heat transfer factor "j" was calculated using the formulas presented in appendix A. Since the tube temperatures at a particular zone were not the same, the

9

hottest tube temperature and link temperature of the zone were averaged. This average temperature was used as the tube temperature in equation (7), appendix A. Using this method of the analysis, the "worst case" j factor was determined for the core inlet, middle, and exit zones. The data plots show an inlet and middle zone performance of somewhat less than predicted and an exit zone performance matching the predicted curve. This indicates that uniform flow distribution through the core was not achieved until near the core exit. The uneven flow distribution is of no consequence at the inlet and middle core zones since the lower gas temperatures at these areas prevent the tubes from exceeding the exit tube temperatures. The data plots also show that as the core Reynolds number increases (increasing flow rate), the j factors for the inlet and middle zones approach the predicted curve. It should be noted that if all tube and link temperatures in a zone were averaged to determine the average tube temperature, the calculated j factors would have fallen very close to the predicted curve. Therefore, the average overall heat transfer performance of the heat source was as predicted.

The friction factor (f) was also calculated using the formulas presented in appendix A. The data plot shows a very close agreement with the predicted curve. Since the calculated "f" takes into account the inlet and exit cone losses, the design assumption that these were negligible was apparently valid.

Figure 10 is a plot of gas flow rate versus the difference in temperature between the hottest tube in a given zone and the gas temperature at the zone. The gas temperature at the middle zone was calculated assuming a linear gas temperature rise through the core in the flow direction. This plot shows the same trend as figure 9. The exit-zone tube-to-gas temperature difference was not affected by gas flow rate as much as in the other two zones. Also, the Δt for all zones tended to flatten out as the flow rate was increased. This plot indicates that care should be taken in operating the heat source at low flowrates. It is possible that with higher heat source inlet temperatures and low gas flow rates, the middle zone tube temperatures could exceed the exit tube temperatures.

Since, for the conditions tested, the heat source core hot spot always occurred at the exit zone, figure 11 has been included in this report. This figure is a plot of the hottest tube temperature in the exit zone as a function of heat source outlet gas temperature. The straight line tube temperature to gas temperature relationship is typical for the uniform flow distribution that was experienced in this zone.

10

The heat source efficiency has been presented as a function of gas flow rate and heat source outlet temperature in figure 12. The efficiency (thermal output/electrical input) presented in the figure reflects the effectiveness of the heat source insulating material and the heat losses through the mounting points and electrical and instrumentation ports. The heat losses are pre-dominantly affected by the containment vessel temperature (or outlet gas temperature). At the high gas flow rates (high power) the heat losses become less significant when compared to the power input. The efficiency curves for the 1250° F and 1650° F outlet gas temperature conditions converge as the power input level is increased. The electric power input to the heat source was measured while the heat source was under set-point control. As a result a true steady-state electrical input power was difficult to determine. This accounts for the data point scatter that can be seen in the figure.

The heat source overall percentage pressure drop ($\Delta PX100/P_{in}$) is presented in figure 13 as a function of gas flow rate. Since the pressure losses were very low, they were difficult to measure accurately. The data has been plotted as recorded and represents a very low overall pressure drop for the flow rates tested. At 1.7 lbs/sec krypton gas flow and 56 psia inlet pressure, the measured pressure drop was .11 #/in^2. The percentage pressure loss ($\Delta PX100/P_{in}$) was 0.20 percent for this condition.

CONCLUDING REMARKS

The heat source was operated at various power levels up to 60 kilowatts electrical and at krypton gas flows from .4 to 1.7 lbs/sec. The performance of the unit is summarized as follows:

(1) During the 225 hours of testing, the heat source performed as designed. The hottest heating element (tube) at the core exit reached a temperature of 1975° F for a heater outlet gas temperature of 1650° F. Since the tube to pin braze has a melting temperature of 2250° F, the 1975° F hot spot was sufficiently below the safe operating temperature limit of the core (2100° F).

(2) The jumper temperatures at the core exit which are adjacent to the tube-pin braze joint consistently ran lower than the tube temperatures. This is an additional safety factor since the 2100° F tube operating limit was based on the melting point of the braze material.

(3) The heat source overall pressure drop was low (.11 #/in^2 at 1.7 lbs/sec gas flow rate and 56 psia inlet pressure). The calculated heat source friction factor which included the losses

through the inlet and exit cones agreed very closely with the friction factors predicted in reference 5.

(4) No problems were encountered when operating the heat source over its design range. However, if the unit is operated at lower flow rates and higher inlet gas temperatures than tested, the tube hot spot could occur in the middle zone of the core.

(5) The electrical and instrumentation ports remained cool (below 200° F) throughout the testing. A small amount of forced air cooling was provided by fans mounted below the ports.

APPENDIX A

HEAT SOURCE PERFORMANCE CALCULATIONS

The heat transfer and pressure drop performance of the heat source were predicted using data from actual tests conducted on a similar core design (ref. 5, fig. 50). The tube spacing in the reference does not represent equilateral spacing of the staggered tube pattern. For ease of construction the heat source core was designed with equilateral tube spacing as indicated in figure 14. This slight change in tube pattern should not affect the heat transfer and friction factor predicted in reference 5.

The following is a list of assumptions made in predicting the heat source performance for steady state operation:

(1) The "j" factor is assumed to be constant throughout the core (uniform flow distribution).

(2) All tubes in the tube bundle are supplying equal amounts of heat into the gas. (All phases have equal resistance-R.)

(3) The temperature of a single tube in the core is constant over its 12-inch length.

(4) Radiation losses from the tube bundle to the containment vessel are negligible. (All electrical input to the heat source is transferred to the gas.)

(5) The inlet and exit cones on the containment vessel do not contribute significantly to the overall heat source pressure drop.

Heat Transfer

In an electric heat source of this type, the electrical power input to the tube bundle must be transferred to the gas, otherwise the tubes will increase in temperature until they are destroyed. The heat transfer performance calculation is therefore aimed at predicting the temperatures at which the tubes will operate. The conditions considered were gas flow rate, power input, and desired outlet gas temperature. The following method was used to predict the tube temperature in the core at any point along the flow path:

13

First determine the desired total thermal input to the gas using

$$q = W C_p \ (t_2 - t_1) \tag{1}$$

Assuming a heat source efficiency (thermal power out/ electrical power in) of .9

$$Q = q/.90 \tag{2}$$

The electrical energy dissipated to the gas by each tube was determined by

$$Q_t = Q/498 \text{ tubes} \tag{3}$$

The local gas Reynolds number was calculated for the tube or tube row of interest using

$$N_{R_\ell} = GD/\mu_\ell \tag{4}$$

Note: Local fluid properties can be determined by assuming a linear temperature rise across the heat source in the flow direction. The heat source has 40 rows of tubes in the flow direction and all tubes within a given row are assumed to be exposed to the same gas temperature. The inlet gas temperature (t_{in_ℓ}) to a particular tube or tube row can be calculated by:

$$t_{in_\ell} = t_1 + \left[((t_2 - t_1)/40) \times (\text{Row No.}-1) \right] \tag{5}$$

The heat transfer factor (j) corresponding to the Reynolds number in (4) was taken from reference 5, figure 50.

Since $j = N_{ST} \ (N_{PR})^{2/3}$

$$h_\ell = j \ GC_p \ (C_p \mu_\ell / k_\ell)^{-2/3} \tag{6}$$

The local log mean temperature difference between the tube and the gas flowing across the tube can be found as follows:

Since $\Delta T_{LM_\ell} = Q_t / h_\ell A_t$

and $\Delta T_{LM_\ell} = (t_t - t_{in_\ell}) - (t_t - t_{out_\ell}) / \log_e \dfrac{t_t - t_{in_\ell}}{t_t - t_{out_\ell}} \tag{7}$

14

where $t_{out_\ell} = t_{in_\ell} + \left(\dfrac{t_2 - t_1}{40}\right)$ (8)

Equation (7) can be solved for the tube temperature (t_t) since it is the only unknown.

Pressure Drop

The heat source pressure drop was calculated using the friction factor data in reference 5, figure 50. The basic equation for predicting the pressure drop of heat exchangers where the gas flow is normal to tube banks is given in reference 5 as:

$$\Delta P = G^2 V_1/2g_c \left[(1+\sigma^2)\left((V_2/V_1)-1\right) + f(A/A_c)(V_m/V_1)\right] \quad (9)$$

$$\underbrace{\text{flow}}_{\text{acceleration}} + \underbrace{\text{core}}_{\text{friction}}$$

Many of the above parameters are constant for a particular core geometry. Applying the constants to equation (9) for the heat source geometry the equation reduces to:

$$\Delta P = W^2 V_1/8.64 \left[1.134\left((V_2/V_1)-1\right)+134 f(V_m/V_1)\right] \quad (10)$$

Since the gas velocity in the inlet and exit cones of the containment vessel is extremely low at the Brayton system maximum flow condition (<10 ft/sec), pressure losses through them were considered negligible.

Electrical Resistance

It was stated earlier that the heat source core consisted electrically of three separate resistors (phases). To determine the desired resistance of each phase, the following were considered:

    a. voltage sources available
    b. heater power input capability desired
    c. line current limitations

From the above a heater power input capability of 30 kilowatts at 208 volts per phase was selected. To achieve this a phase resistance of 1.5 ohms was required. After considering various ways of electrically connecting the Inconel tubes and various tube wall thicknesses, a series connection of all tubes within a phase was

selected. A tube wall thickness of .065 inch was also selected.
With this configuration the phase resistance of the heater can be
calculated from:

$$R = 7900 \rho_N + 33,200 \rho_I \qquad (11)$$

The above formula takes into account the Inconel tube and nickel
jumper resistance. (See ref. 4 and 6 for values of ρ.) The
nickel lead resistance and braze resistance (Inconel tube to nickel
pin) has been considered negligible.

Stress

Stress calculations were performed for various sections of the
heater core and containment vessel. The results showed that the
highest stresses occur in the containment vessel at the cylindrical
section. At 50 #/in^2 differential pressure from the inside to out-
side of the containment vessel, the maximum stress is in the order
of 1000 #/in^2. For Inconel 600, this represents a factor of safety
of 2 based on the stress to produce rupture in 10,000 hours at
1600° F.

REFERENCES

1. Wood, James C.; et al.: Preliminary Performance Characteristics of a Gas-Bearing Turboalternator. NASA TM X-1820, 1969.

2. Wong, Robert Y.; Klassen, Hugh A.; Evans, Robert C.; and Winzig, Charles H.: Preliminary Investigation of a Single-Shaft Brayton Rotating Unit Designed for a 2- to 10-kilowatt Space Power Generation System. NASA TM X-1869, 1969.

3. Desmon, L. G.: Brayton Cycle Radiant Gas Heating System. Rep. ER-2062, Solar Div., International Harvester Co. (NASA CR-72575), Apr. 1969.

4. Anon.: Engineering Properties of Inconel Alloy 600. Tech. Bull. T-7, Huntington Alloy Products Div., International Nickel Co., Inc.

5. Kays, William M.; and London, A. L.: Compact Heat Exchangers. McGraw-Hill Book Co., Inc., 1958.

6. Anon.: Handbook of Huntington Alloys. Huntington Alloy Products Div., International Nickel Co., Inc.

7. Kohl, Walter H.: Joining of Metals by Brazing. Materials and Techniques for Electron Tubes. Reinhold Publ. Corp., 1960, Ch. 12.

TABLE I

HEAT SOURCE MATERIALS

Containment vessel	1/2" Inconel 600 plate
Baffles and supports	1/8, 1/4, & 3/8" Inconel 600 plate
Header frame	1/16" Inconel 600 sheet
Electrical and instrumentation ports	2" schedule 10 Inconel 600 pipe
Power leads and terminals	A - nickel
Tube pins	A - nickel
Tube jumpers	A - nickel
Metal ends of power lead feed-throughs	A - nickel
Metal ends of instrumentation feed-throughs	Monel
Ceramic headers	Alumina 95
Thermocouple insulators	Alumina 95
Power lead insulators	Alumina 95
Power lead feed-through (ceramic)	Alumina 95
Instrumentation feed-through (ceramic)	Alumina 95
Nickel pin to Inconel tube braze	35% cobalt, 65% paladium (ref. 7)
Nickel power lead stud to feed-through braze 316 SS thermocouple sheath to feed-through braze	50% silver 15.5% copper 15.5% zinc 16% cadmium 3% nickel
Nickel pin to nickel jumper	Tungsten inert gas weld

Nickel Pins Brazed
into Heater Tubes.

Ceramic Header

Heater Tubes

Nickel Jumpers

CM
0 1 2 3 4 5

Figure 1 - Partially Assembled
Heater Core.

Gas Flow

Jumper Thermocouple

Exit Phase

Middle Phase

Inlet Phase

Tube Thermocouple

Power Lead
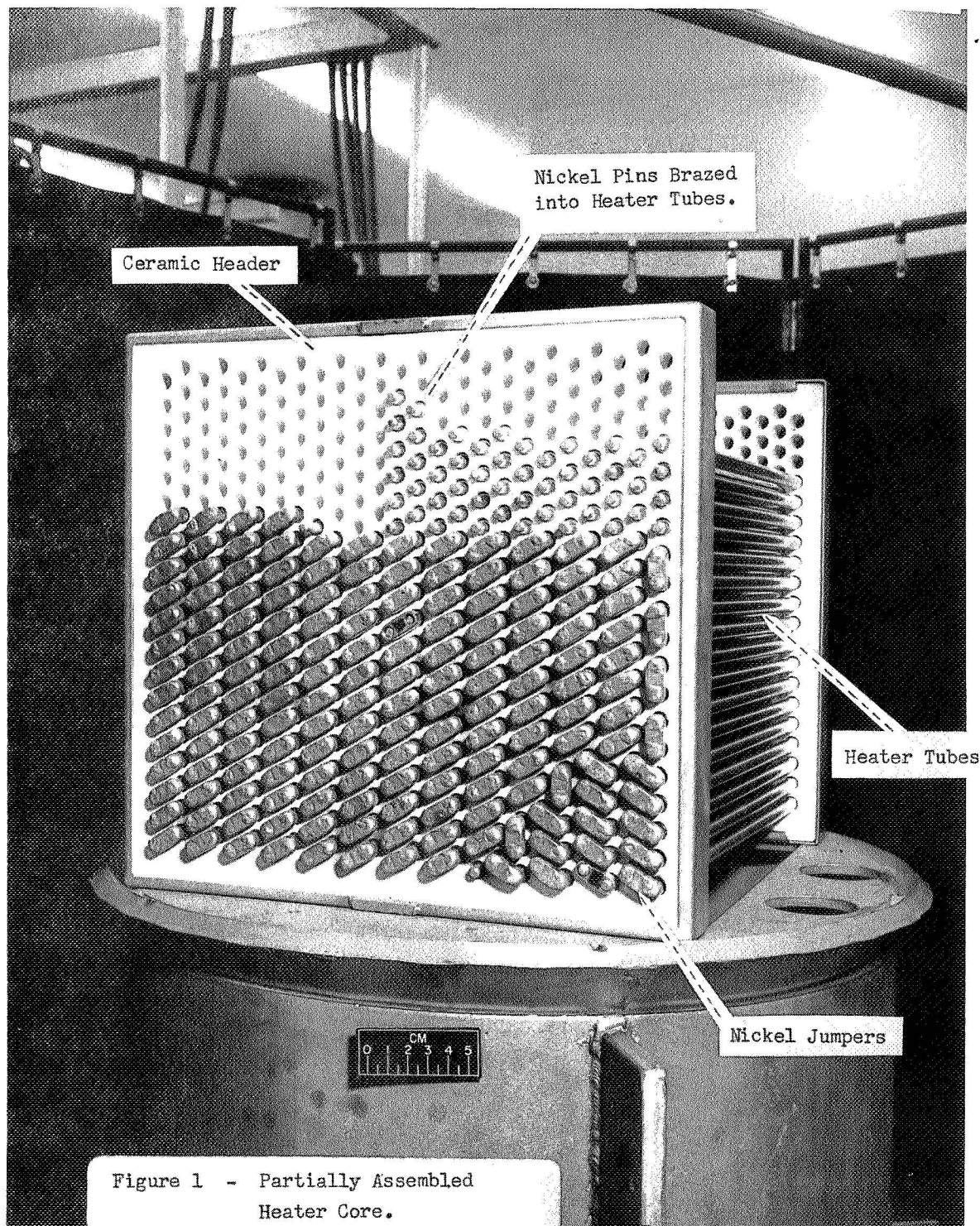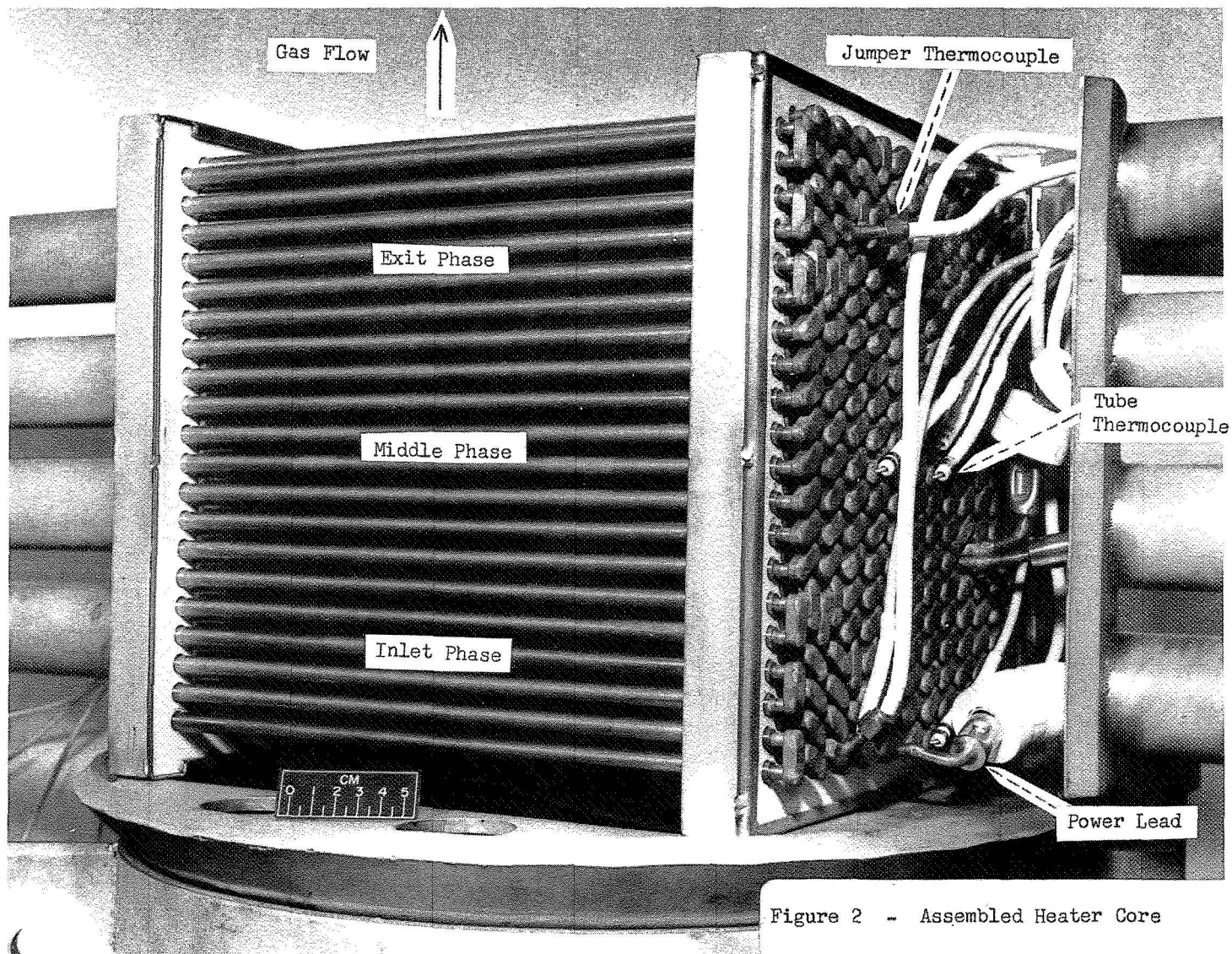
Figure 2 — Assembled Heater Core

Outgassing Holes

Power and
Thermocouple Ports

Containment
Vessel

Baffle

Figure 3 - Heater Core Top View Prior
to Outlet Cone Installation.
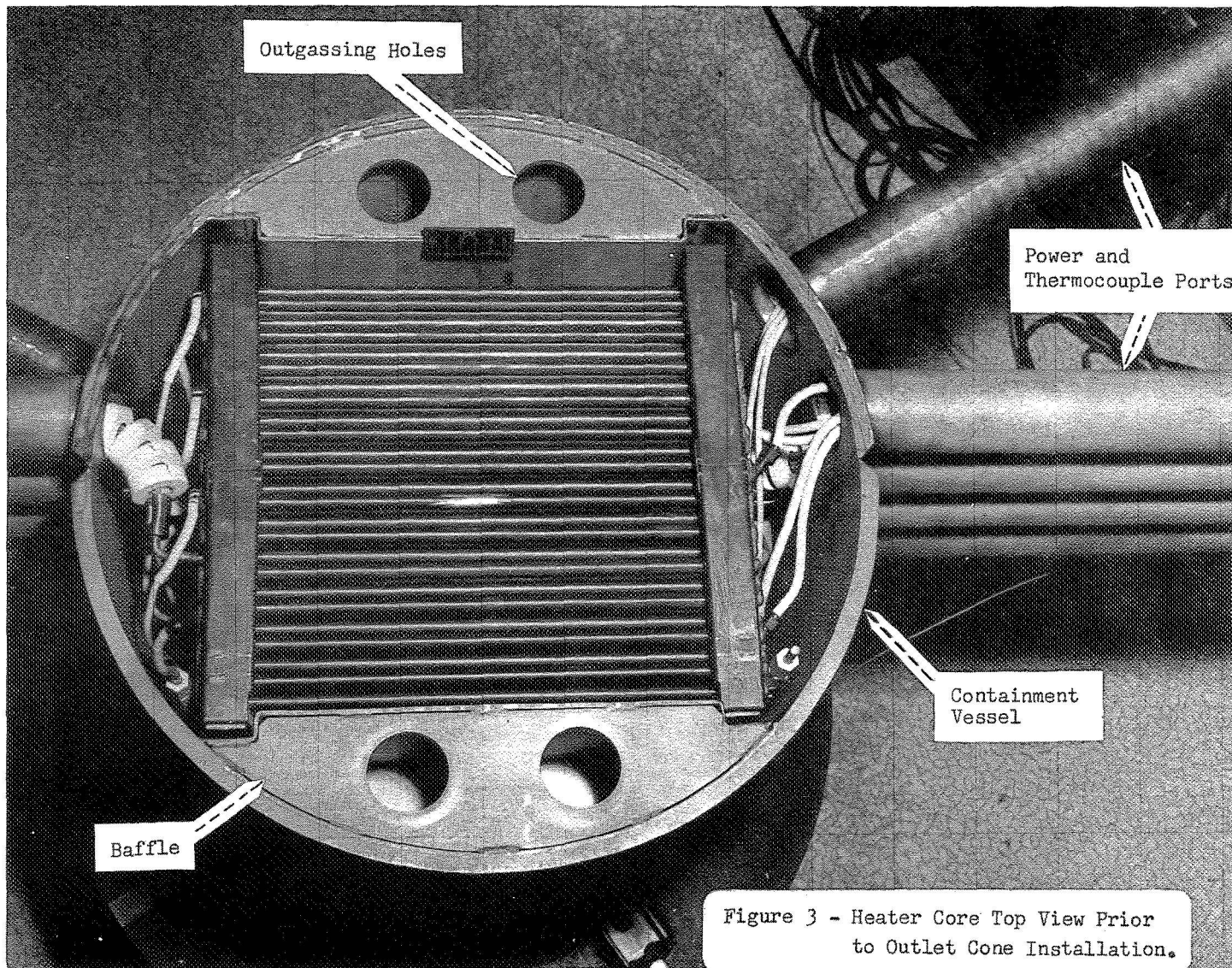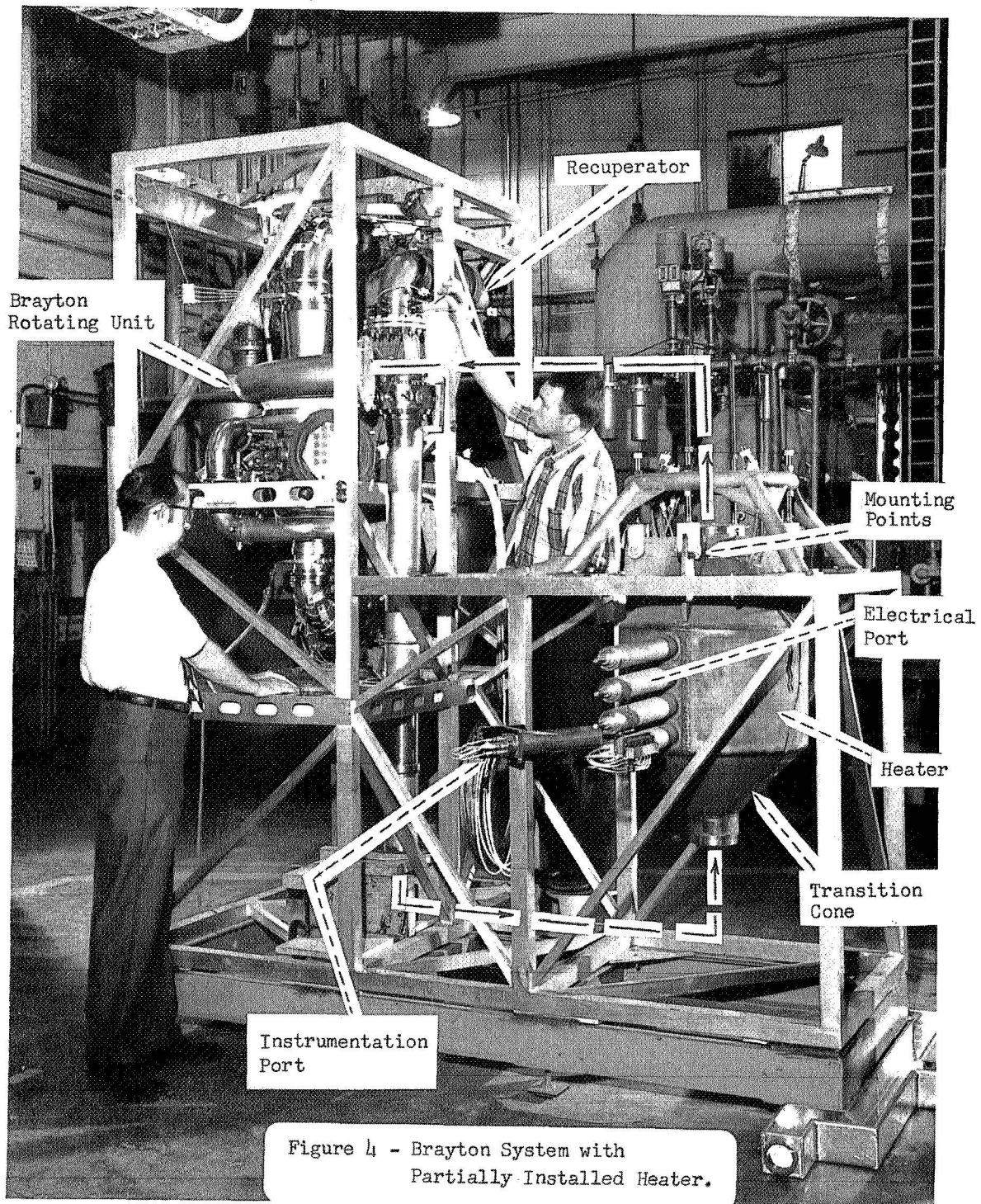
Figure 4 – Brayton System with Partially Installed Heater.

Nickel Connector

Ceramic Insulators

Stranded Nickel Leads

Crimp

Figure 5 - Heat Source Power Leads.
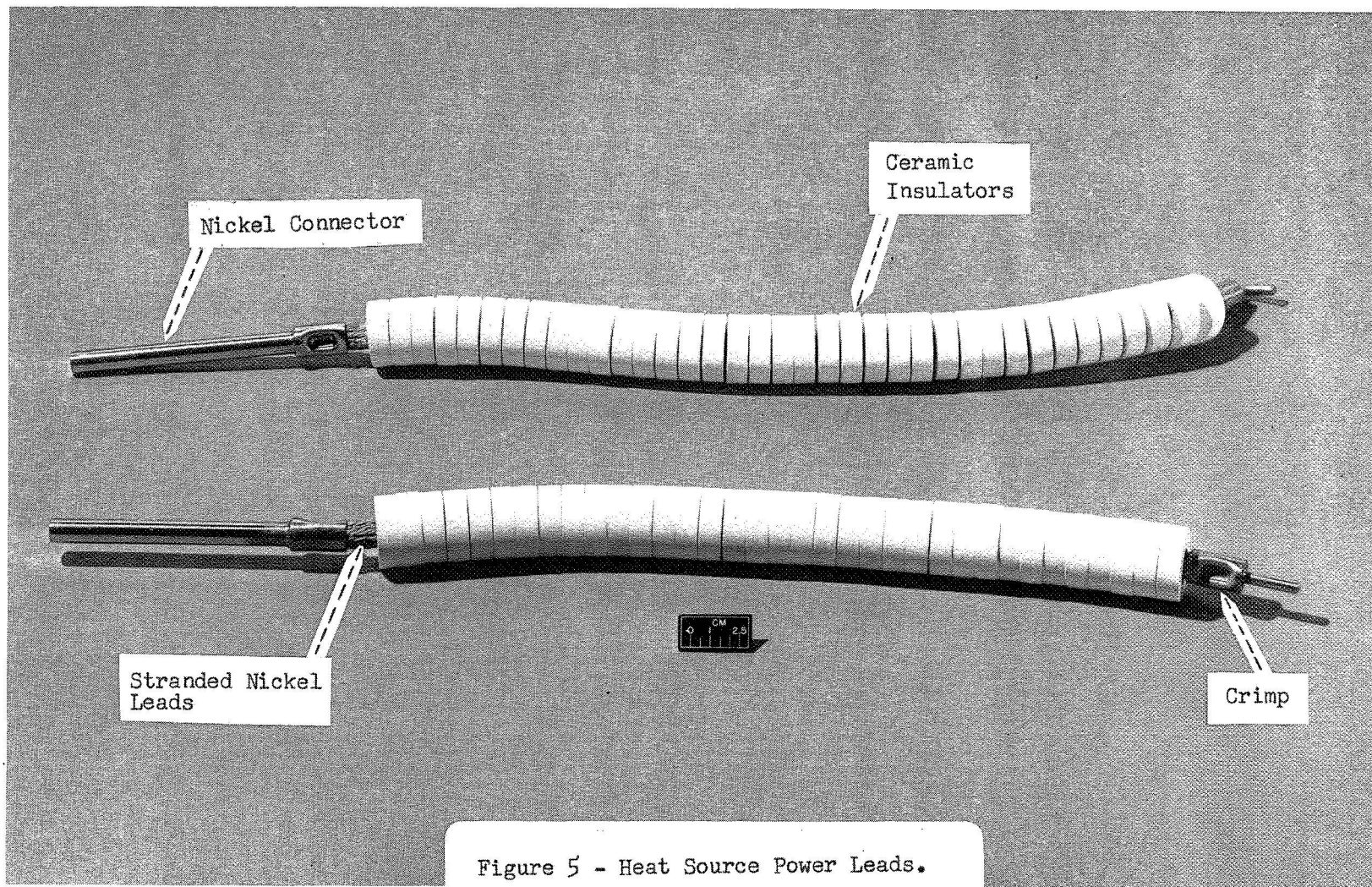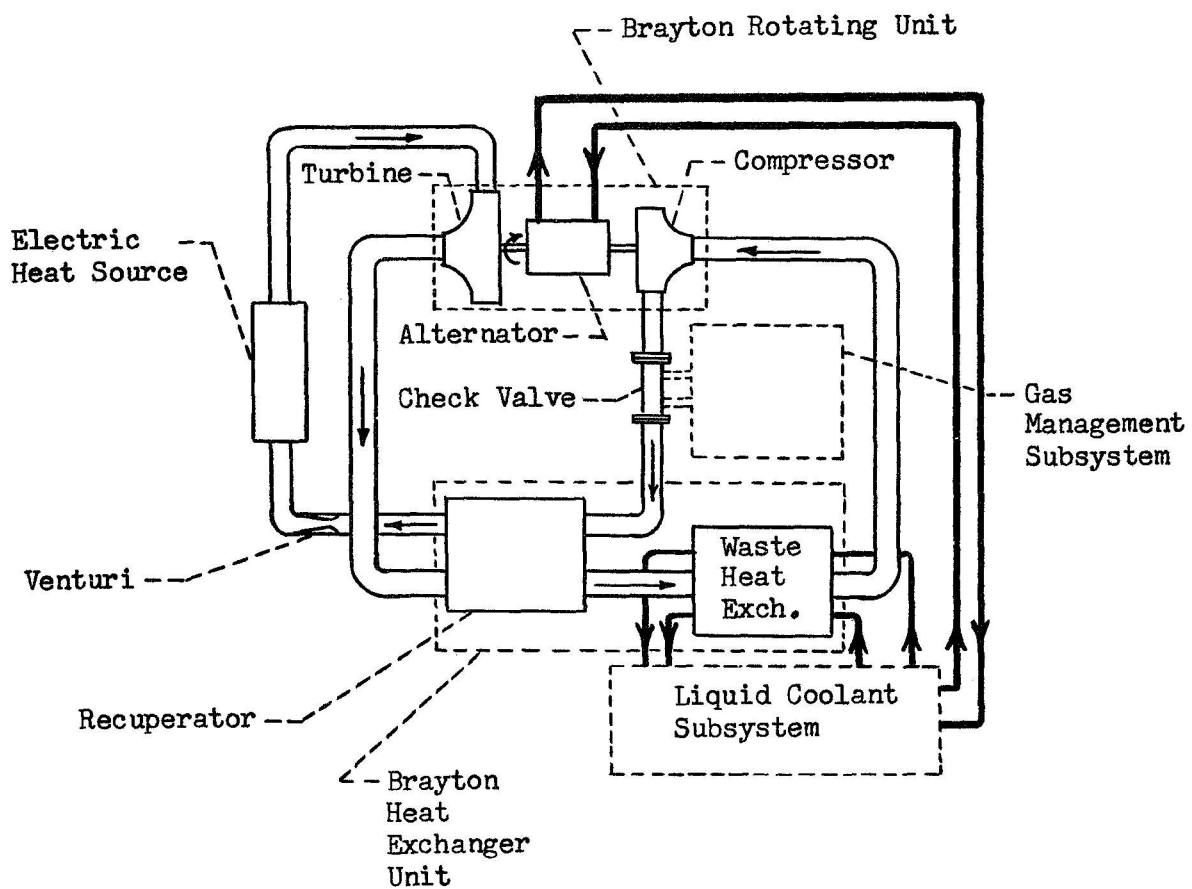
Figure 6 - NASA - Brayton Power Conversion System Schematic.

Brayton Heat
Exchanger Unit

Pressure
Instrumentation

High Temperature
Quartz Insulation

Uninsulated
Ports

Thermocouple
Leads

Gas Flow

Braided
Power Lead

Figure 7 - Heater Installed
and Insulated.

1745°F   1822°F

1761°F

1783°F   1936°F

1928°F

A-A
(EXIT ZONE)

1689°F   1705°F

1715°F

1750°F   1560°F

B-B
(MIDDLE ZONE)

1313°F

1371°F   1495°F

1449°F

1499°F

1313°F

C-C
(INLET ZONE)

1655°F

1730°F

140°F

A   A

B   B

C   C

1340°F

1109°F

FLOW
.855
#/SEC.

FIGURE-8

HEAT SOURCE THERMAL MAP FOR 38 KW ELECTRICAL POWER IMPUT CONDITION
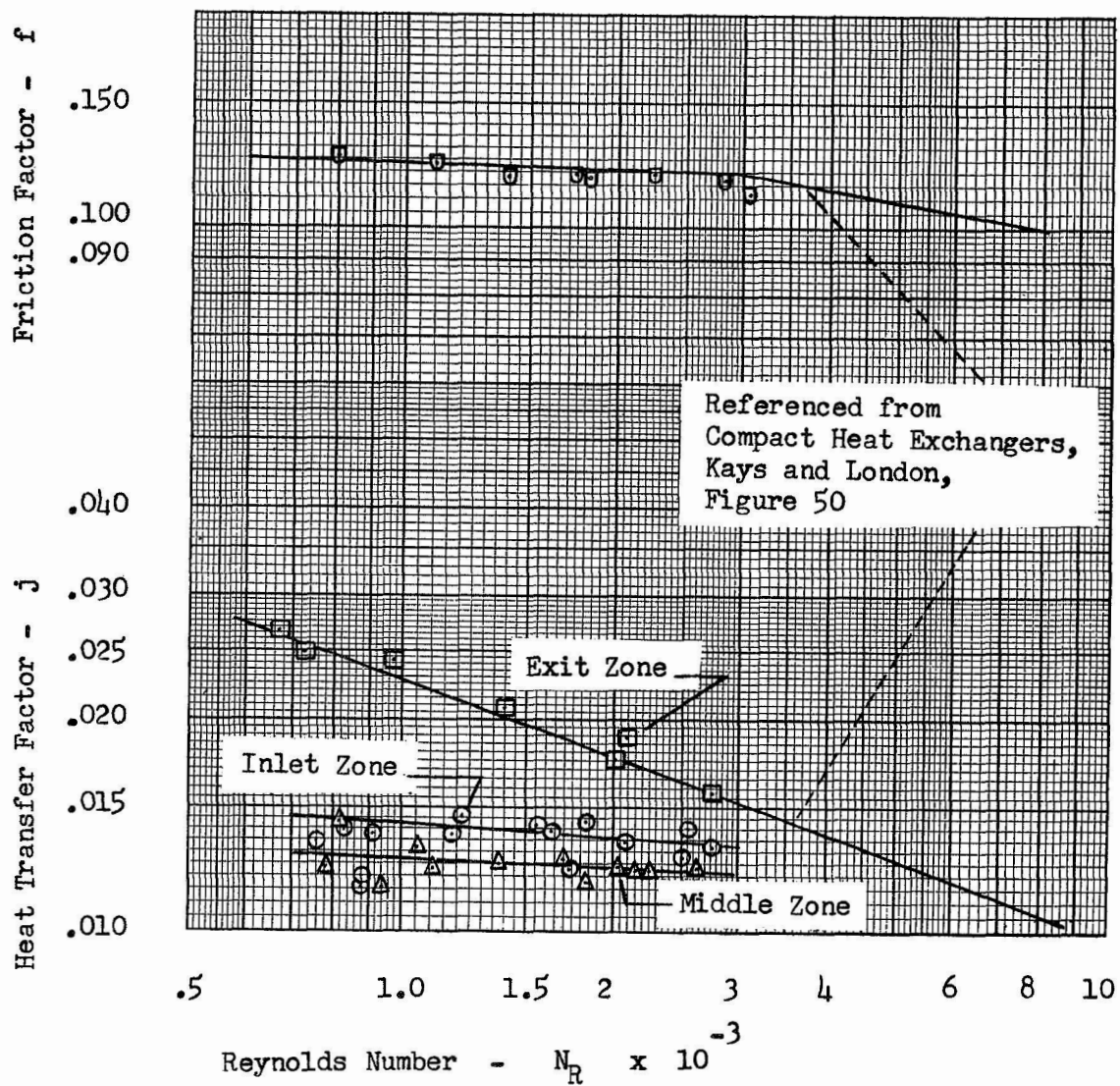
Figure 9 - Comparison of Actual and Predicted Performance
Factors vs. Reynolds Number.
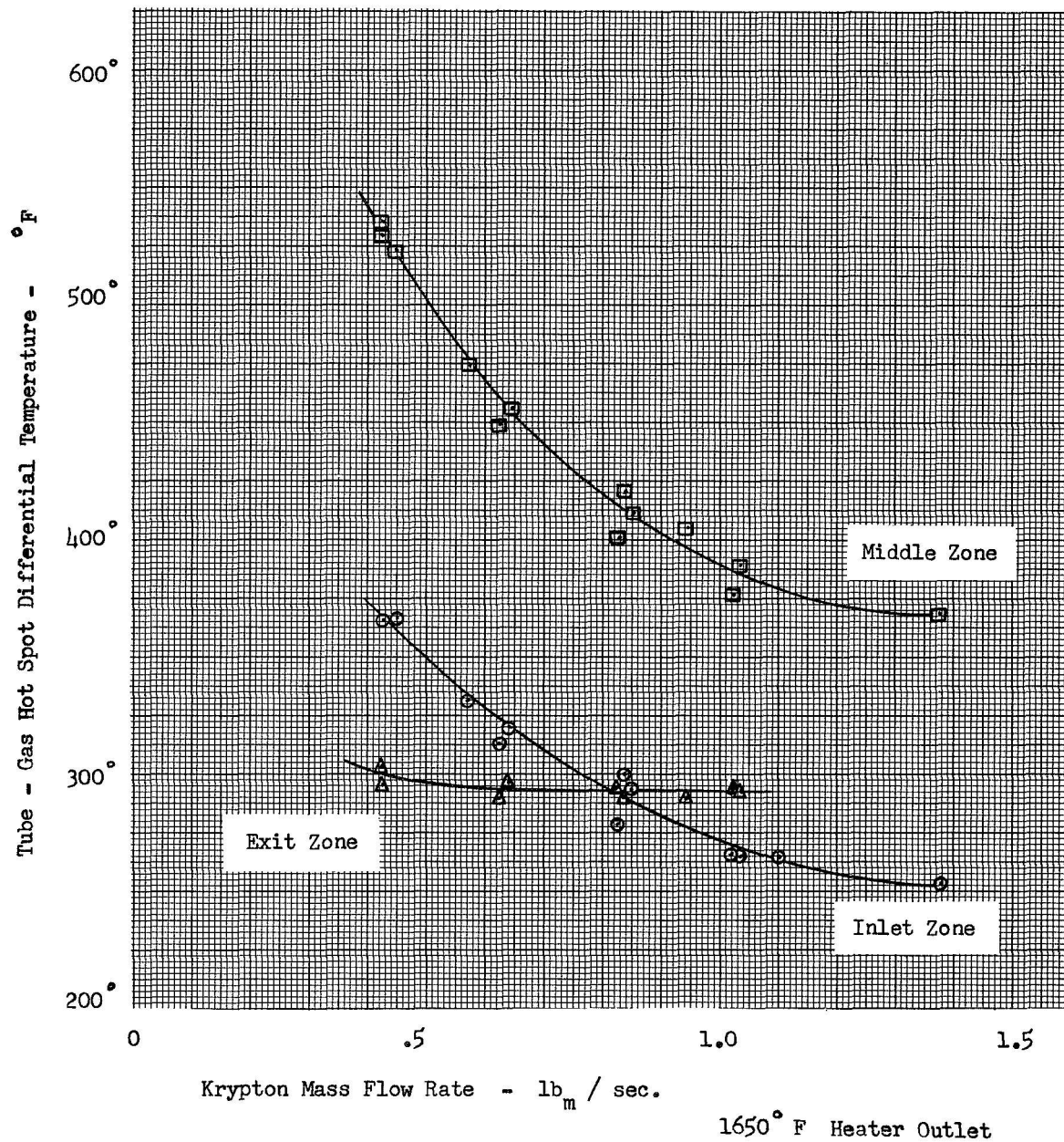
Figure 10 - Effect of Gas Mass Flow Rate on Tube to Gas Hot Spot
Differential Temperature.
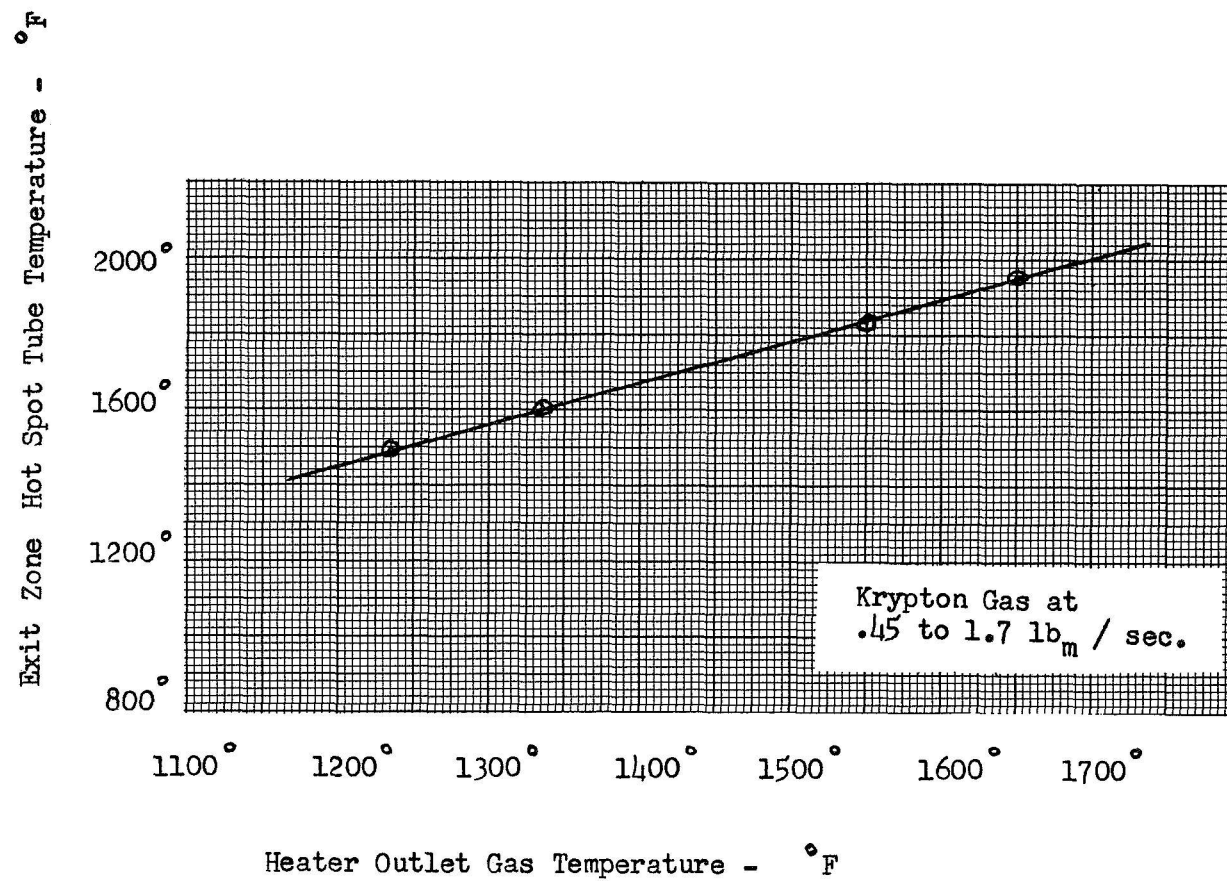
Figure 11 - Effect of Heater Outlet Gas Temperature on
Exit Zone Hot Spot Tube Temperature.
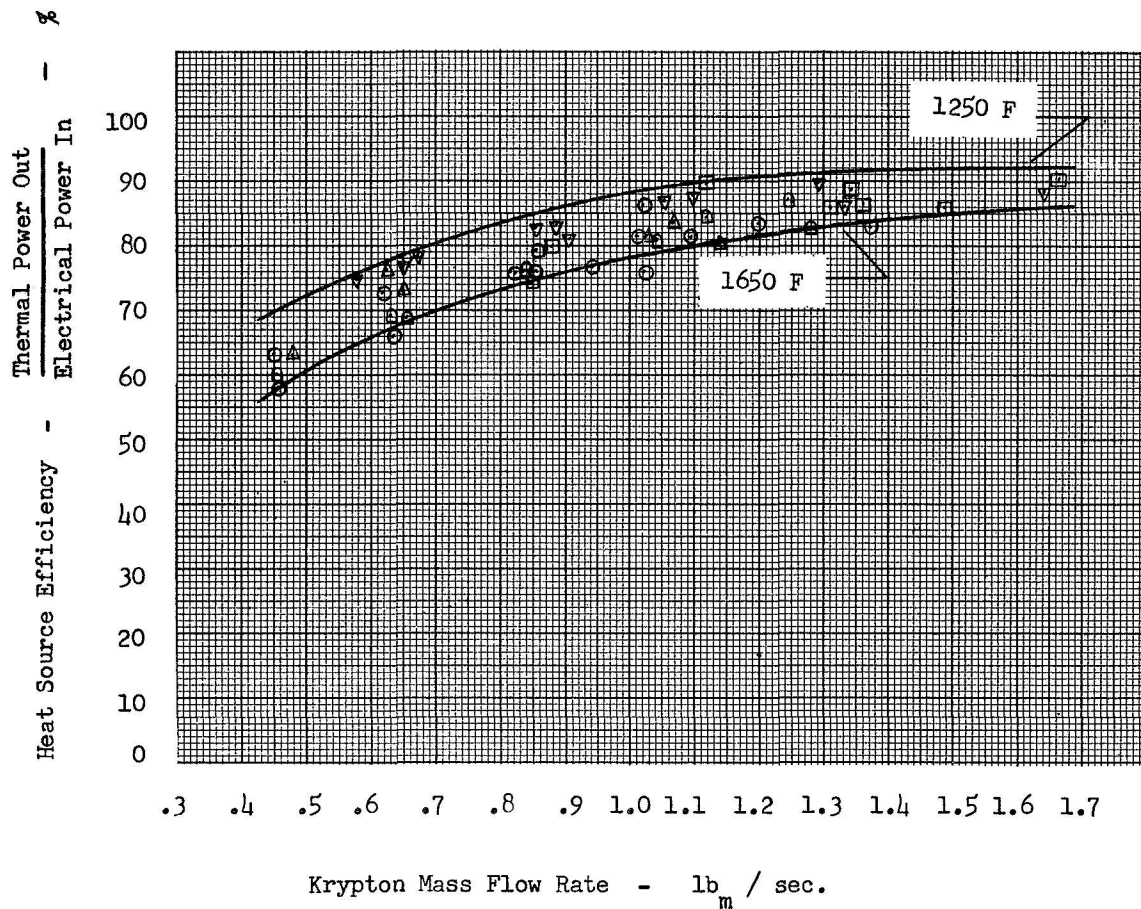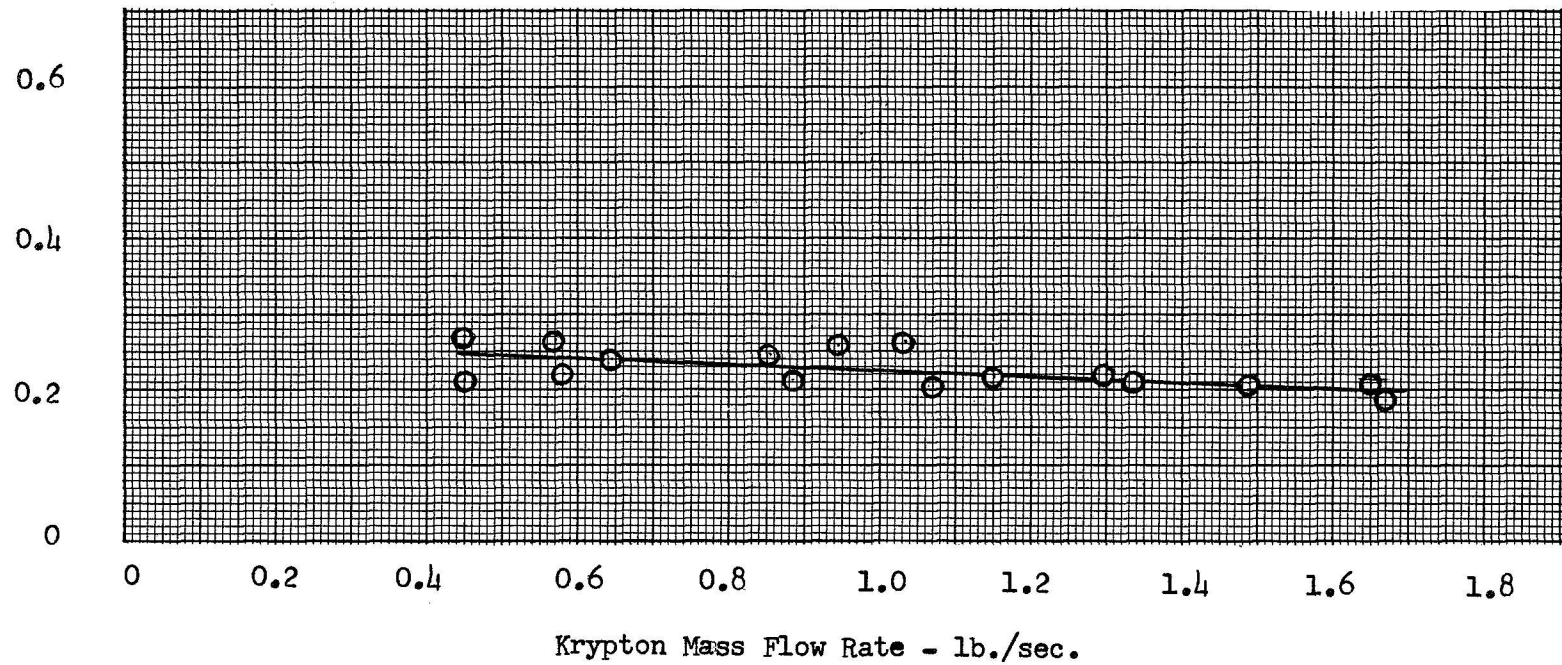
Figure 12 - Effect of Gas Outlet Temperature on
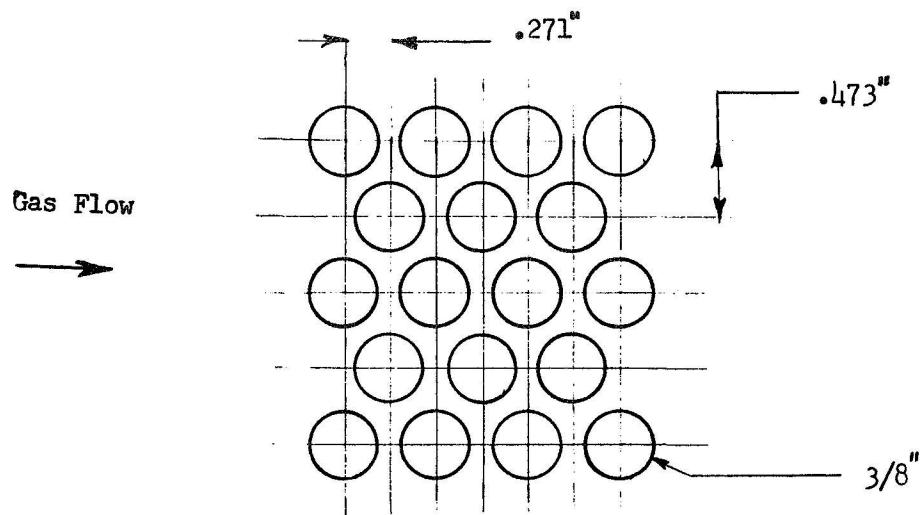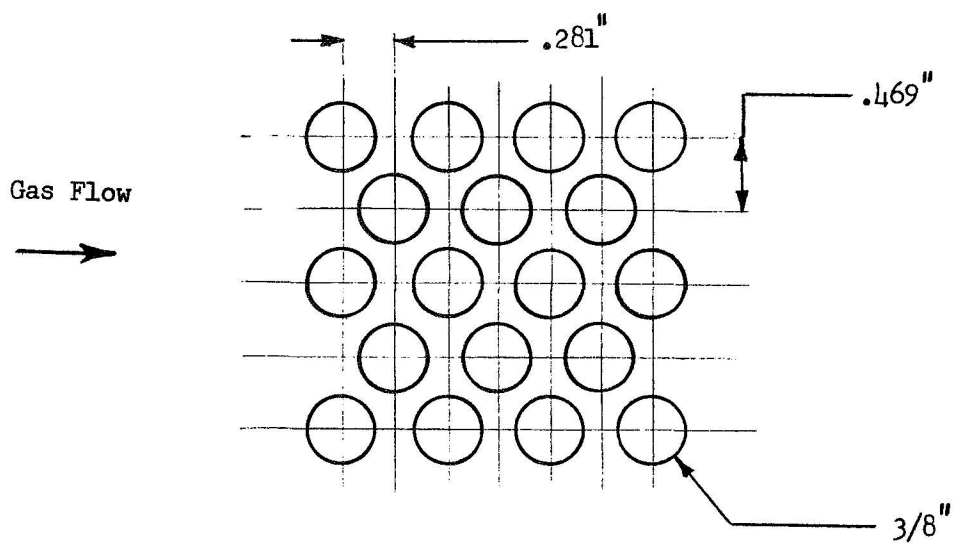Heat Source Efficiency.

Figure 13 - Heat Source Percentage Pressure Loss vs. Gas Mass Flow Rate

Actual Core Geometry

Reference Core Geometry
(Kays and London, Fig. 50)

Figure 14 - Comparison of Actual Core Geometry to Reference
Core Geometry.